

# BRANCHING MEDIAL MODELS FOR CARDIAC SHAPE REPRESENTATION

Hui Sun<sup>1</sup>, Brian B. Avants<sup>1</sup>, Alejandro F. Frangi<sup>2</sup>, Sebastian Ordas<sup>2</sup>, James C. Gee<sup>1</sup> and Paul A. Yushkevich<sup>1</sup>

<sup>1</sup>Departments of Radiology, University of Pennsylvania, Philadelphia, PA, USA

<sup>2</sup> Information and Communication Technologies Department, University Pompeu Fabra, Barcelona, Spain and Networking Center on Biomedical Research - CIBER-BBN, Barcelona, Spain

## ABSTRACT

The cm-rep (continuous medial representation) is a powerful shape representation method that models a 3D object by describing its medial axis (skeleton) and boundary as continuous parametric manifolds. It provides parametrization of the entire interior of the object, which can be used for combined statistical analysis of shape and appearance. This paper extends the cm-rep to more complex shapes with multi-figures, i.e., shapes whose skeletons have branches. Along the branching curves, the equality constraints enforced by the medial geometry are implemented as soft penalties in the deformable model. The remaining small violations are corrected by local adjustments. As a proof of concept, the branching continuous medial representation is applied to a 2-chamber heart model data set consisting of 428 cardiac shapes from 90 subjects. The results show that our model can capture the heart shape accurately.

**Index Terms**— Medial Axis, Branching Medial Model, 2-chamber heart model, Cardiac Thickness Analysis

## 1. INTRODUCTION

Medial axis (skeleton) has the ability to represent shape compactly and to provide global shape features. Therefore, it has a variety of applications in medical imaging analysis field, like shape analysis [1], shape-based segmentation and registration [2]. Medial models describe structures by explicitly defining the medial axis of the structures and deriving boundary geometry from the medial axis. If the structure has a complex shape, i.e., its skeleton can not be described by a single curve (2D) or single sheet (3D), the corresponding medial model is called branching medial model.

There have been efforts to model complex shapes using medial models. Han proposed a “multi-figure” medial model [3] that represents each part of a complex object medially, but does not model the connections between parts in terms of

medial geometry. Rather, it uses surface blending to attach a “child” single-figure medial model to its “parent”. This type of model is very useful when complex objects have a “parent-child” organization of parts (like the hand, with a palm and five fingers), but it is not clear how it can be used to model structures where the parts do not follow such an obvious tree hierarchy, like the heart.

Unlike medial representation (m-rep), where the medial axis is defined by a small set of rich primitives called medial atoms, continuous medial representation (cm-rep) [4] uses continuous parametric manifolds to represent the skeleton and provides parametrization to the entire interior of the model. Recently, there has been work in extending the cm-rep approach to complex objects with branching skeletons. The difficulty of constructing such models arises from the fact that the geometric relationship between the medial axis and the boundary imposes equality constraints that must be satisfied along branching curves. For single-sheet medial models, a Poisson PDE can be used to generate a space of models that satisfy this constraint [4], but this approach does not extend to branching models. Terriberry proposed the first solution to the problem [5]. He uses Catmull-Clark subdivision surfaces to model the skeleton and enforces the equality constraints by locally modifying the skeleton at boundary and branching curve to use an interpolating spline. This solution is very elegant, but it is somewhat limited by the requirement of Catmull-Clark subdivision surfaces with quadrilateral elements being used. To the best of our knowledge, Terriberry’s branching model has not yet been applied to large-scale anatomical modeling.

We were inspired by Terriberry’s demonstration of the fact that the equality constraint required by the medial geometry along branching curve can be enforced by a very local correction. Actually, the constraints only involve the first order derivatives of the functions on the branching curve, and thus can be satisfied by localized adjustment. Based on that, we propose a new way to resolve the problem. We first use soft penalties to obtain solutions that only slightly violate the equality constraints, and then use local corrections to make sure that different parts of the boundary come together.

Our branching medial model is tested on a large scale

---

Medial methodology development is funded by the NIH grant AG027785 and NS061111. We also acknowledge support from Spanish MEC (TEC2006-03617), ISCIII (FIS2004/40676), and CDTI(CENIT-CDTEAM); as well as Dr. Marina Hugué from CETIR - Sant Jordi Cardiovascular Centre (Barcelona, Spain) for kindly providing the cine MR data sets used in this work.

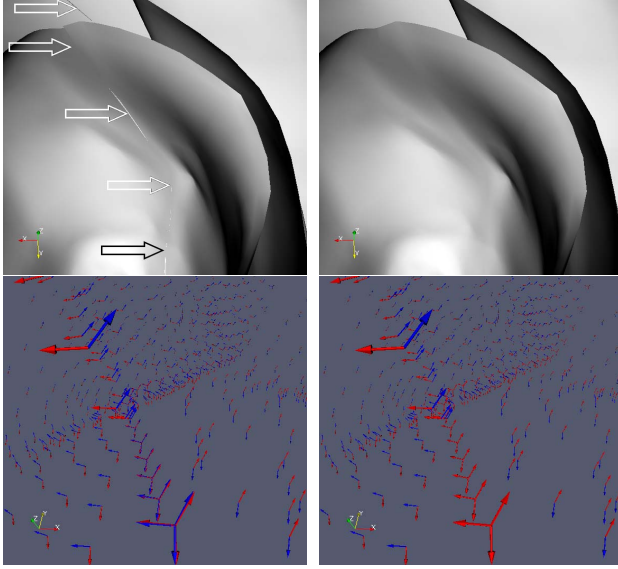


**Fig. 1.** This figure illustrates the result of the deformable model with soft penalties and the effect of local correction. The left column shows the results after deformable fitting with soft penalties. The right column shows the results after local correction. The top row is the model boundary, note that before the correction, there are very tiny seams on the boundary, indicated by the arrows, which disappears after the correction. The bottom row shows the spoke vector field. Note that before the correction, the 6 spokes for the point on medial seam do not match perfectly into 3, but have very small discrepancy within each pair (one red and one blue as a pair), while after the correction only 3 spokes can be observed.

cardiac data set in this paper. Cardiac shape modeling is very useful in many aspects. It provides features for shape analysis and subsequently incorporates statistical shape priors into cardiac image analysis methods, like segmentation [6], which could be very challenging without prior knowledge. The cardiac medial modeling is promising because it explicitly provides thickness information, which is an important global feature. We fit the model to a large data set containing 428 2-chamber heart shapes, and obtained a mean overlap of 91.44%. To the best of our knowledge, this is the first study to apply branching medial model at such a large scale. The robustness of our method is thus demonstrated.

## 2. METHOD

### 2.1. Medial Geometry

We first briefly introduce the terminology and concepts of medial geometry. Given a geometric object  $\mathcal{O}$  in  $\mathcal{R}^3$ , we define a *maximal inscribed ball (MIB)* in  $\mathcal{O}$  as any ball  $\mathcal{B}$  satisfying  $\mathcal{B} \subseteq \mathcal{O}$  and for which there does not exist another ball  $\mathcal{B}'$  such that  $\mathcal{B} \subset \mathcal{B}' \subseteq \mathcal{O}$ . The locus of the centers and radii of all MIBs is called the *skeleton*, or *medial axis* of the object. The skeleton is thus composed of two components: the locus of the centers of all MIBs in  $\mathcal{R}^3$ , which will be referred to as *medial scaffold*, or  $\mathbf{m}$ ; and the locus of radii in  $\mathcal{R}^+$ , which is called the *radial scalar field* or the *thickness field*, or  $R$ .

Please refer to Damon [7] for an extensive study of 3D medial geometry.

The medial scaffold is a *Whitney stratified set* [7], i.e., a collection of manifolds with boundary that are connected along edges. These manifolds will be referred to as *medial manifolds*. The part of their boundaries that is shared by multiple manifolds will be called *medial seam* or *branch curve*, while the part of the boundaries that only belongs to one medial manifold will be called *medial edge*. Giblin and Kimia [8] proved that there are 5 types of points that form the medial scaffold, according to the order and multiplicity of tangency between their MIBs and the boundary of the object. They are: (1) points on the interior of medial manifolds; where the MIB is tangent to the objects boundary at two points. (2) points on medial edges, where the MIB is tangent to the boundary at one point; (3) points on medial seams, where the MIB is tangent to the boundary at three points with first-order contact with the boundary; (4) points at medial seam-edge intersections; and (5) points at medial seam-seam intersections.

### 2.2. Equality Constraints Along Medial Edges and Seams

In the deformable medial model, the user specifies  $\mathbf{m}$  and  $R$  as some mesh/function/surface and then deforms them to fit image data. The deformable medial model approach leverages the idea of *inverse skeletonization*[4], where the *skeleton* of an object is defined first and the objects boundary is derived analytically from the skeleton. Because the topology and configuration of the skeleton is predefined, this approach guarantees the consistency of the skeleton within a cohort, which makes population study possible. The key difficulty lies on the well-posedness of the inverse skeletonization problem, that is, given arbitrary connected surface patches  $\mathbf{m}$  and arbitrary positive field  $R$ , the  $\{\mathbf{m}, R\}$  pair may not form the skeleton of any subject; rather, inverse skeletonization is only possible for the  $\{\mathbf{m}, R\}$  pairs who satisfy a set of equality and inequality constraints enforced by the medial geometry.

Let's first introduce the geometric relationship between the skeleton and object boundary. For the first type of points on the medial scaffold, the MIBs are tangent to the object boundary at two points  $\mathbf{b}^+$  and  $\mathbf{b}^-$ , they can be derived analytically from  $\mathbf{m}$  and  $R$ :

$$\mathbf{b}^\pm = \mathbf{m} + R\vec{\mathbf{U}}^\pm \quad (1)$$

$$\vec{\mathbf{U}}^\pm = -\nabla_m R \pm \sqrt{1 - \|\nabla_m R\|^2} \vec{\mathbf{N}}_m, \quad (2)$$

where  $\vec{\mathbf{N}}_m$  is the unit normal vector of the medial manifold at point  $\mathbf{m}$ ,  $\vec{\mathbf{U}}^\pm$  are unit length vectors orthogonal to  $\partial\mathcal{O}$  at  $\mathbf{b}^\pm$ , and  $\nabla_m$  is the Riemannian gradient of  $R$  on the medial manifold. The vectors  $R \cdot \vec{\mathbf{U}}^\pm$ , i.e, the vectors pointing from the center of a MIB to the corresponding boundary tangency points, are called *spokes*.

Near a medial edge, the two spokes will get closer and closer to each other, collapsing to a single vector once the medial edge is reached. This ensures the boundary of the object

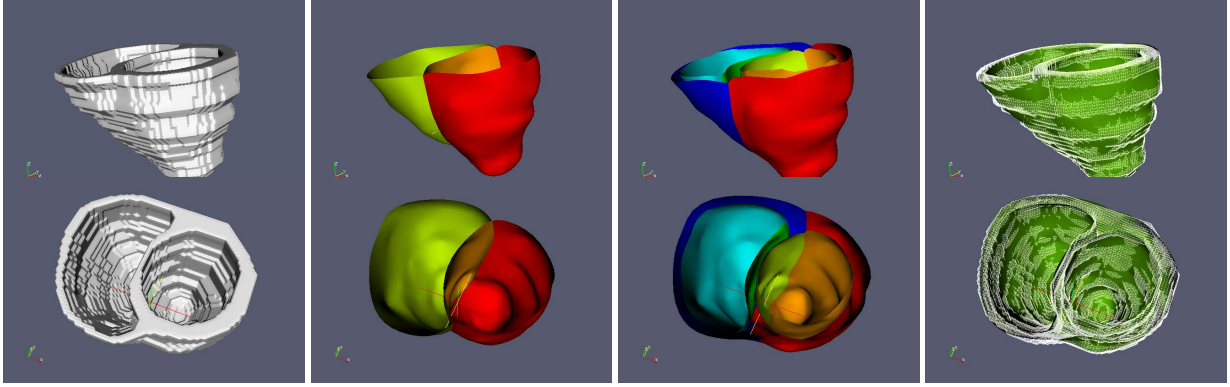


**Fig. 2.** An example of fitting the 2-chamber heart shape. The top row and bottom row are shown from different viewpoints. The first column is the binary segmentation of the left and right ventricles. The second column is the fitted medial model, using different color to identify medial manifolds. The third column is the medial boundary: each medial manifold generates two pieces of boundary, and those boundary patches connect seamlessly. The fourth column overlays the model boundary, which is shown as green surfaces, on the binary segmentation, which is shown as white wireframe.

is closed. The corresponding equality constraint is:

$$\|\nabla_m R\| = 1. \quad (3)$$

Accordingly, the soft penalty for violating this constraint can be put as:

$$(\|\nabla_m R\| - 1)^2 \quad (4)$$

Points on the medial seam belong to three medial manifolds  $\mathbf{m}^i \{i = 1, 2, 3\}$ . When approaching the medial seam, the 6 spokes pair up according to certain order and pairs of spokes are getting closer and closer, collapsing to 3 vectors once the medial seam is reached. This ensures that different boundary patches generated from the 3 medial manifolds come together to form the boundary of an object. Assume the three patches are oriented so that  $\vec{\mathbf{U}}^{i,+} = \vec{\mathbf{U}}^{i\oplus 1,-}$  ( $\oplus$  denotes additional modulo 3) at the seam, then the constraints are:

$$\nabla_m^{i\oplus 2} R - \nabla_m^{i\oplus 1} R = \sqrt{1 - \|\nabla_m^i R\|^2} \vec{\mathbf{N}}_m^i. \quad (5)$$

With some algebra, the equality constraints above can be written as

$$\frac{\partial R}{\partial \vec{\mathbf{s}}_i} + \sqrt{1 - \left(\frac{\partial R}{\partial \vec{\mathbf{t}}}\right)^2} \vec{\mathbf{N}}_m^{i\oplus 1} \cdot \vec{\mathbf{N}}_m^{i\oplus 2} = 0, \quad (6)$$

where  $\vec{\mathbf{t}}$  is the tangent vector of the seam curve, and  $\vec{\mathbf{s}}_i = \vec{\mathbf{t}} \times \vec{\mathbf{N}}_m^i$ , which is tangent to the medial manifold  $\mathbf{m}^i$  and orthogonal to the seam curve. Accordingly, the soft penalty for violating this constraint can be put as:

$$\left(\frac{\partial R}{\partial \vec{\mathbf{s}}_i} + \sqrt{1 - \left(\frac{\partial R}{\partial \vec{\mathbf{t}}}\right)^2} \vec{\mathbf{N}}_m^{i\oplus 1} \cdot \vec{\mathbf{N}}_m^{i\oplus 2}\right)^2. \quad (7)$$

Along the medial seam there is another inequality constraint. The angle between any two medial manifolds should be smaller than  $\pi$ . This ensures that each spoke is located between the two medial manifolds it belongs to.

At the seam-edge intersection,  $\|\nabla_m^i R\|$  equals to 1 for the medial manifold whose edge is crossing the intersection,

and the other two manifolds will have angle  $\pi$  (actually they merge into one manifold at the intersection point).

There are several more inequality constraints that the  $\{\mathbf{m}, R\}$  pair need to satisfy, like  $\|\nabla_m R\| < 1$  for all type 1 points and the Jacobian constraint to prevent local self-intersection of the boundary. Please refer to [4] for a more detailed description.

Because of the complicated topology of the medial scaffold, it is far easier to use non-parametric surface representations to describe medial manifolds. Loop subdivision surface [9] are especially well suited because of their triangular elements and simplicity. The triangular control meshes for Loop subdivision surface can be recursively refined by inserting a vertex into each edge in the parent-level according to a set of subdivision rules. The mesh in our model is subdivided up to a sufficiently accurate level and the model boundary is reconstructed on it. Boundary reconstruction from the skeleton in Eqs 1-2 requires only up to first order derivative information. We calculate them according to [10], which involves one ring of neighbors for each vertex. The soft penalties are computed on all vertices along medial seam and medial edge and their average values will be used in the objective function of the deformable model. In practice, we find that the vertices on the medial seam should have at least valence 3 to get enough freedom to satisfy the branching constraints.

The deformable branching medial models are fitted to the segmented binary images in a fashion that is quite similar to [4]. But here the objective function in the deformable model includes the soft penalties to enforce constraints at medial edges and seams, also we added a regularization term which controls the quality of the medial mesh by penalizing big and small angles in the triangles.

We then use a brute-force local adjustment to ensure that the boundary generated from the skeleton is closed. Along the medial edge and medial seam, each pair of spokes will be given the mean value of that pair, so that all parts of the boundary will connect seamlessly. We found out that as long

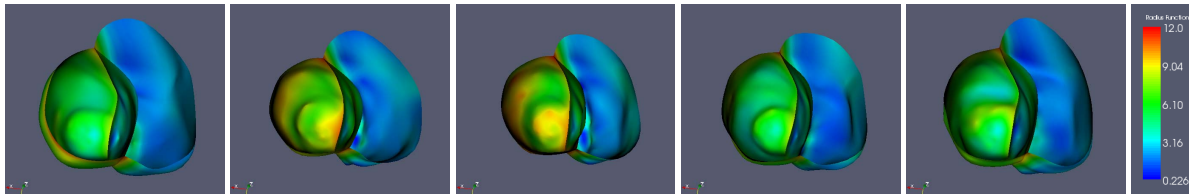


**Fig. 3.** The medial model of the heart in different phases of a cardiac cycle. The medial scaffold are colored by thickness. From left to right, the five phases plotted are ED (End Diastole), MS (Mid Systole), ES (End Systole), D1 (Diastole 1) and D2 (Diastole 2).

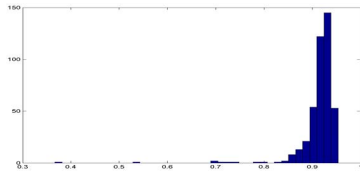


**Fig. 4.** The histogram of the Dice overlap coefficients for all 428 fitted branching medial models.

as the soft penalties are enforced on the geometry at medial edges and seams, the correction that's needed is tiny in practice. Fig 1 shows the medial geometry before and after the brute-force correction around the medial seam. While this is not as elegant as Terriberry's interpolation scheme, is very effective in practice.

### 3. RESULT

The data set used here contains 90 MR studies from CETIR Sant Jordi Centre (Barcelona, Spain), which consist of both healthy subjects and patients suffering from common Cardiovascular pathologies. The acquisition parameters were: TR: 3.75 4ms, TE: 1.5-1.58 ms, FA: 45, slice thickness: 8C10 mm, slice size:  $256 \times 256$  pixels, resolution:  $1.56 \times 1.56$  mm and FOV:  $400 \times 300$  mm<sup>2</sup>, on a General Electric CVI 1.5 T MR facility. Expert segmentations were manually drawn on the endocardial left ventricle and right ventricle borders, and the epicardial border of the whole heart to construct a 2-chamber heart model which usually includes 8-12 slices from the base to the apex. Different phases of the cardiac cycle were segmented. Overall 428 heart shapes are used in the experiment.

The proposed branching medial model is fitted to the 428 manual segmentation of 2-chamber heart model in a multi-resolution fashion. Fig. 2 gives an example of the fitting. Fig. 3 shows the fitted medial model of the heart in 5 different phases of one cardiac cycle. Fig 4 shows the histogram of the Dice coefficient. The overall mean Dice overlap coefficient for all 2-chamber heart shapes is  $91.44(\pm 4.48)\%$ . Note that the manual segmentation voxel size is quite big (8-10mm between slices), one would expect the smooth surface approximation of the discrete segmentation to be less accurate. Also, because the whole structure is thin, the boundary surface area is large and the overlap ratio is brought down a bit.

### 4. FUTURE WORK

The medial model of the heart is very promising: the thickness information provided by the medial model is potentially

a descriptive feature in shape analysis and a strong prior in learning based segmentation. We plan to adopt our method to the current learning based left ventricle segmentation framework [6] to further improve its accuracy and robustness.

### 5. REFERENCES

- [1] M. Styner, G. Gerig, J. Lieberman, D. Jones, and D. Weinberger, "Statistical shape analysis of neuroanatomical structures based on medial models.," *Med Image Anal*, vol. 7, no. 3, pp. 207–20, Sep 2003.
- [2] S. M. Pizer, P. T. Fletcher, S. Joshi, A. Thall, J. Z. Chen, Y. Fridman, D. S. Fritsch, A. G. Gash, J. M. Glotzer, M. R. Jiroutek, C. Lu, K. E. Muller, G. Tracton, P. Yushkevich, and E. L. Chaney, "Deformable m-reps for 3D medical image segmentation.," *International Journal of Computer Vision*, vol. 55, no. 2, pp. 85–106, Nov 2003.
- [3] Qiong Han, Stephen M. Pizer, Derek Merck, Sarang Joshi, and Ja-Yeon Jeong, "Multi-figure anatomical objects for shape statistics.," in *Information Processing in Medical Imaging*, 2005, pp. 701–712.
- [4] Paul A. Yushkevich, Hui Zhang, and James Gee, "Continuous medial representation for anatomical structures.," *IEEE Trans Med Imaging*, vol. 25, no. 2, pp. 1547–1564, December 2006.
- [5] Timothy B. Terriberry and Guido Gerig, "A continuous 3-d medial shape model with branching.," in *MICCAI*, 2006.
- [6] Hans C. Van Assen, Mikhail G. Danilouchkine, Alejandro F. Frangi, Sebastián Ordás, Jos J.M. Westenberg, Johan H.C. Reiber, and Boudewijn P.F. Lelieveldt, "Spasm: A 3D-ASM for segmentation of sparse and arbitrarily oriented cardiac MRI data.," *Medical Image Analysis*, vol. 10, no. 2, pp. 286–303.
- [7] J. Damon, "Determining the geometry of boundaries of objects from medial data.," *International Journal of Computer Vision*, vol. 63, no. 1, pp. 45–64, 2005.
- [8] P. Giblin and B. Kimia, "A formal classification of 3D medial axis points and their local geometry.," in *IEEE Computer Society Conference on Computer Vision and Pattern Recognition*, 2000, pp. 566–573.
- [9] C. Loop and T. DeRose, "Generalized b-spline surfaces of arbitrary topology.," in *Computer Graphics (ACM SIGGRAPH Proceedings)*, 1990, pp. 347–356.
- [10] Guoliang Xu, "Discrete laplace-beltrami operators and their convergence.," *Comput. Aided Geom. Des.*, vol. 21, no. 8, pp. 767–784, 2004.